

Tribovoltaic Nanogenerators Based on MXene-Silicon Heterojunctions for Highly Stable Self-Powered Speed, Displacement, Tension, Oscillation Angle, and Vibration Sensors

Xiongxin Luo, Lindong Liu, Yi-Chi Wang, Jiayu Li, Andy Berbille, Laipan Zhu,* and Zhong Lin Wang*

Tribovoltaic nanogenerators (TVNGs), an emerging high-entropy energy harvesting technique, present great features such as low matching resistance, high current density, and continuous output performance. Here, an MXene layer and a semiconducting silicon wafer are assembled into a tribovoltaic nanogenerator (named MS-TVNG). The output peak current of the MS-TVNG reaches up to 22 μA for a P-type (0.1–0.5 $\Omega\text{ cm}$) silicon wafer under a normal force of 4.56 N and a sliding speed of 2 m s^{-1} . Owing to the unique metal characteristics of the MXene layer, the performance is superior to those previously reported TVNGs using traditional metals. The layered structure of MXene endows the real-time MS-TVNG with outstanding wear-resistance and stable output properties. The performance of the MS-TVNG can be tuned by the doping type and concentration of the silicon wafer, as well as by the pressure and the relative sliding speed between two friction surfaces. The MS-TVNG has proven to be a solid foundation for high-performance self-powered speed sensors and has excellent potentials for applications in displacement, tension, oscillation angle, and vibration detection.

efficiency to convert random, low-frequency mechanical energy and other forms of high-entropy energy, promising to form distributed power supplies.^[2] They are also envisaged as self-powered sensors to detect instantaneous pulsed mechanical stimuli.^[3] Direct-current (DC) output nanogenerators have the potential to greatly extend their application to real-time sensing for consecutive mechanical motions.^[4] Recently, progress has been achieved in low-frequency energy harvesting using tribovoltaic nanogenerators (TVNGs), devices consisting in metal/semiconductor,^[5] P-N semiconductor,^[6] metal/conducting polymer,^[7] aerogel/silicon^[8] or liquid/semiconductor^[9] dynamic junctions. The sliding Schottky nanocontact generates DC signal due to the diffusion and drift motions of non-equilibrium carriers on the microscopic scale.^[10] The concept of tribovoltaic effect

and its basic mechanisms were proposed in 2019, which was described as follows.^[11] During friction, a bindington, the energy quantum when two atoms form a bond, will be released, which excite electron-hole pairs across the sliding interface. Electron-hole pairs are then separated and expelled out of the junction attributed to the built-in electric field, thus generating continuous DC current. Only the drift motion of carriers plays a decisive role on the macroscopic scale. Although many power

1. Introduction

With the rapid development of artificial intelligence, big data, and the Internet of Things, human's demands for miniaturized and distributed power sources have increased dramatically.^[1] Compared with traditional electromagnetic generators (EMGs) and solar cells, piezoelectric nanogenerators (PENGs) and triboelectric nanogenerators (TENGs) demonstrate better

X. Luo, L. Liu, Y.-C. Wang, J. Li, A. Berbille, L. Zhu, Z. L. Wang
CAS Center for Excellence in Nanoscience
Beijing Key Laboratory of Micro-nano Energy and Sensor
Beijing Institute of Nanoenergy and Nanosystems
Chinese Academy of Sciences
Beijing 101400, P. R. China
E-mail: zhulaipan@binn.cas.cn; zlwang@binn.cas.cn

X. Luo, L. Zhu, Z. L. Wang
Center on Nanoenergy Research
School of Physical Science and Technology
Guangxi University
Nanning 530004, P. R. China

Y.-C. Wang, J. Li, L. Zhu, Z. L. Wang
School of Nanoscience and Technology
University of Chinese Academy of Sciences
Beijing 100049, P. R. China

A. Berbille
CAS Center for Excellence in Nanoscience
National Center for Nanoscience and Technology
Beijing 100190, P. R. China

Z. L. Wang
School of Material Science and Engineering
Georgia Institute of Technology
Atlanta, GA 30332, USA

 The ORCID identification number(s) for the author(s) of this article can be found under <https://doi.org/10.1002/adfm.202113149>.

DOI: 10.1002/adfm.202113149

generation devices based on TVNGs have been proposed, one very desirable application has not been widely explored yet. TVNGs have great potentials to design high-performance self-powered mechanical sensors.

Recently, the novel 2D-layered transition metal carbide/carbonitride MXenes (such as $\text{Ti}_3\text{C}_2\text{T}_x$, Ti_2CT_x , Nb_2CT_x , V_2CT_x , Ti_3CNT_x , and Mo_2CT_x) have attracted wide attention due to their unique structures and electronic properties.^[12] They are usually produced by selectively etching the A layer from metal conductive layered MAX phases (M = transition metals, A = main group elements, and X = C/N). During the etching process, the A atoms are replaced by different functional groups, yielding MXene nanosheets with hydroxyl, oxygen, or fluorine groups on the surface.^[13] Therefore, the MXene displays a highly hydrophilic surface, with diverse chemical properties and tunable properties without losing the metal conductivity of transition metal carbides.^[14] Such combinational properties are difficult to achieve in traditional 2D atomic crystals such as graphene, layered transition metal dihalides and layered double hydroxide.^[15] Thus, MXene has been demonstrated in applications such as light-to-heat conversion, energy storage, and electrostatic shielding.^[12b,14,16]

Here, we use the $\text{Ti}_3\text{C}_2\text{T}_x$ MXene and semiconductor silicon wafer to construct a tribovoltaic nanogenerator (named MS-TVNG). Similar to traditional metals, the MXene can produce a stable and continuous DC output by rubbing it against silicon wafers, and the peak output current of the MS-TVNG can reach up to 22 μA . The MS-TVNG presents outstanding wear-resistance and energy output stability over those made by traditional metals. In addition, the output current of the MS-TVNG increases linearly when increasing the applied pressure and sliding speed. Therefore, a novel principle for self-powered speed, displacement, tension, oscillation angle, and vibration sensors is proposed.

2. Results and Discussion

The $\text{Ti}_3\text{C}_2\text{T}_x$ MXene nanosheets usually present as black powders. Therefore, tableting appeared to be an appropriate approach to prepare the MXene films into a friction layer for the MS-TVNGs. The fabrication steps of the MXene sliders are shown in **Figure 1a**. The MXene-based slider was prepared by dispersing the MXene powders on a copper tape and then

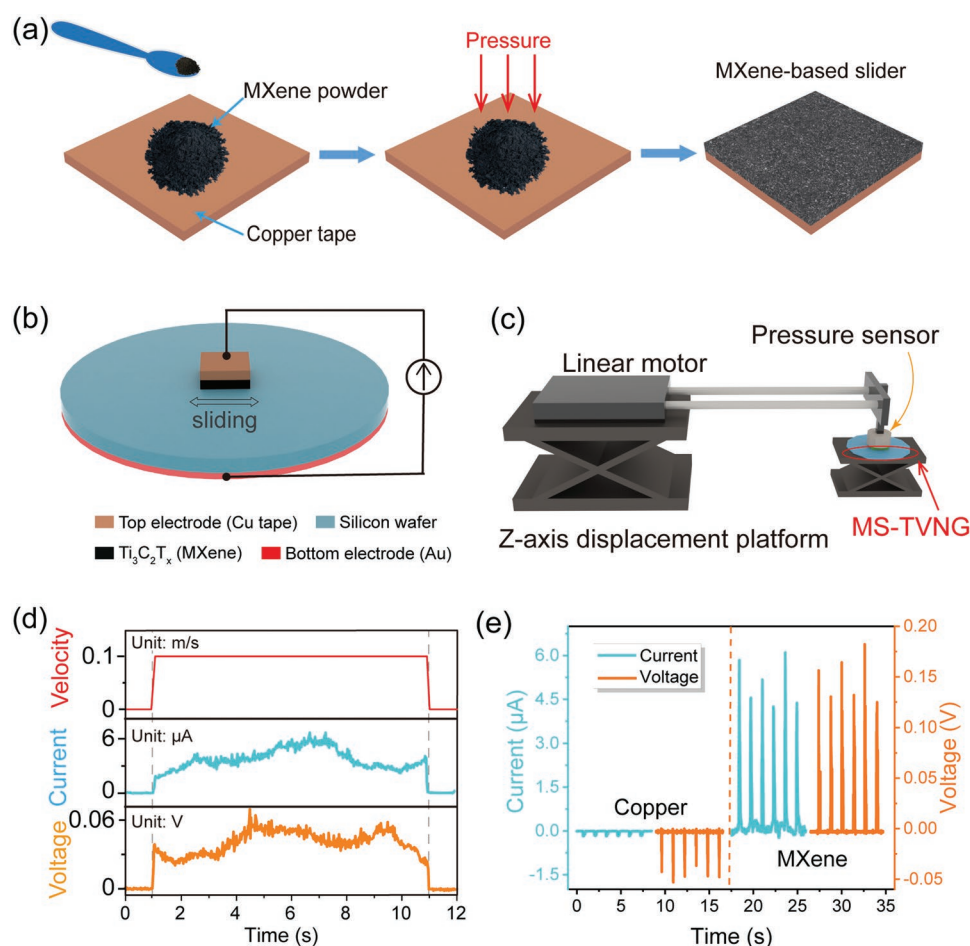


Figure 1. Illustration of the device structure, experimental setup, and electric output characteristics of the MS-TVNG. a) Step-by-step fabrication processes of the MXene-based slider. b) Testing principle of electrical performance and schematic structure of the MS-TVNG. c) Schematic of the experimental setup. d) DC output open-circuit voltage and short-circuit current signals of the MS-TVNG. e) Comparison of the output short-circuit current and open-circuit voltage using a copper slider and the MXene film slider, respectively.

exerting a high pressure (20 MPa) to attach the MXene powder tightly onto the copper tape. The MXene-based slider thus formed includes a top electrode copper and an MXene film. After etching the natural oxidized layer on the surface of the silicon wafer with hydrofluoric acid, an approximately 50 nm thick Au bottom electrode was sputtered using magnetron sputtering. Finally, an external circuit is used to connect the bottom and top electrodes. The device structure is shown in Figure 1b. The MXene film can make good contact with the surface of the silicon wafer, and be slid under an external force using a linear motor-based experimental set-up (Figure 1c). The linear motor is employed to provide a horizontal sliding movement. Two z-axis displacement platforms are used as supports to adjust the pressure at the sliding interface. A pressure sensor is installed between the linear motor and the slider to measure the applied pressure. The MS-TVNGs are capable of generating a DC electrical output when rubbing MXene film against a semiconductor silicon wafer, as shown in Figure 1d. The output signals are continuous and can respond effectively to changes in sliding speed. This is probably due to the MXene films can maintain the metal conductivity of transition metal carbides which could lead to high output performances. To illustrate the superior performance of the MS-TVNGs, the electrical output of a Cu-based and an MXene-based TVNGs under the same experimental conditions (where the area of the upper copper electrode, the normal force, the sliding speed, and the type of silicon wafer are $1.5 \times 1.5 \text{ cm}^2$, 4.56 N, 2 m s^{-1} , and N-type ($20\text{--}40 \ \Omega \cdot \text{cm}$), respectively) are compared, as shown in Figure 1e. The MXene-based TVNG generates more than 30 times higher output current ($5.8 \ \mu\text{A}$) compared with a Cu-based TVNG ($0.18 \ \mu\text{A}$).

The powder X-ray diffraction (XRD) pattern and the Raman spectra of the as-prepared MXene film, shown in Figure 2a,b,

are in agreement with previous reports.^[17] Figure 2c presents a bright-field transmission electron microscopy (BF-TEM) image of the MXene nanosheets, which exhibits a clear layered structure. A perfect single crystallinity of the MXene is demonstrated by the selective area electron diffraction (SAED) pattern in the inset of Figure 2c. The energy dispersive X-ray (EDX) spectrum mapping (Figure S1, Supporting Information) and the high-angle annular dark-field scanning transmission electron microscopy (HAADF-STEM) image (Figure S2, Supporting Information) unveil a uniform distribution of Ti, F, O, and C elements. More importantly, the MXene powder can be pressed tightly together and can construct a relatively flat film simply by employing a tablet press, as shown in the SEM image in Figure 2d. Moreover, the inset of the SEM image shows the MXene retained the layered structure after pressing. The firmly composed yet layered microstructure of MXene is of great significance to reduce friction losses and maintain a stable electric output. Traditional TVNGs are usually composed of P-N junction,^[6a] metal/semiconductor,^[5a] metal/perovskite,^[18] or metal/conducting polymer. Relatively large friction losses in materials with low Young's modulus are inevitable when rubbing against materials with higher Young's modulus, which would cause a sharply declined performance of the TVNGs.^[19] Optical micrographs of the silicon surfaces corresponding to the Cu-based and MXene-based TVNGs under the same fatigue testing conditions are shown in Figures 2e–f, respectively. The observation confirms that the MXene-based TVNG shows more uniform and gentle scratches. That is, the MXene nanosheets here can greatly enhance the wear-resisting property of the triboelectric interface over Cu-based TVNGs. Two possible reasons account for the enhanced wear-resisting property. One is that a small amount of MXene powders falls off the film during

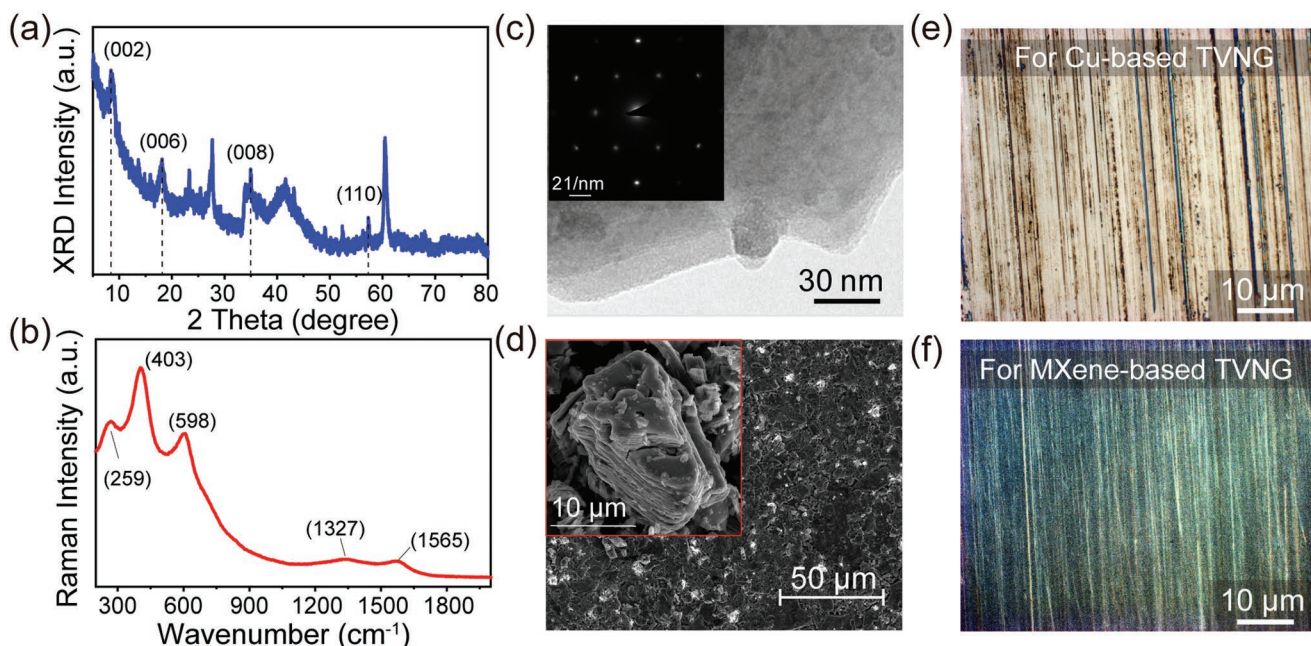


Figure 2. The microstructure of the layered MXene used for TVNGs. a,b) XRD pattern and Raman spectra of the MXene film. c) TEM image of the MXene nanosheets, where the inset is a SAED pattern of the MXene nanosheets. d) SEM images of the used MXene film, where the inset shows the layered structure after pressing. e,f) Optical micrographs of silicon wafers after friction with Cu-based (e) and MXene-based (f) films under the same testing conditions.

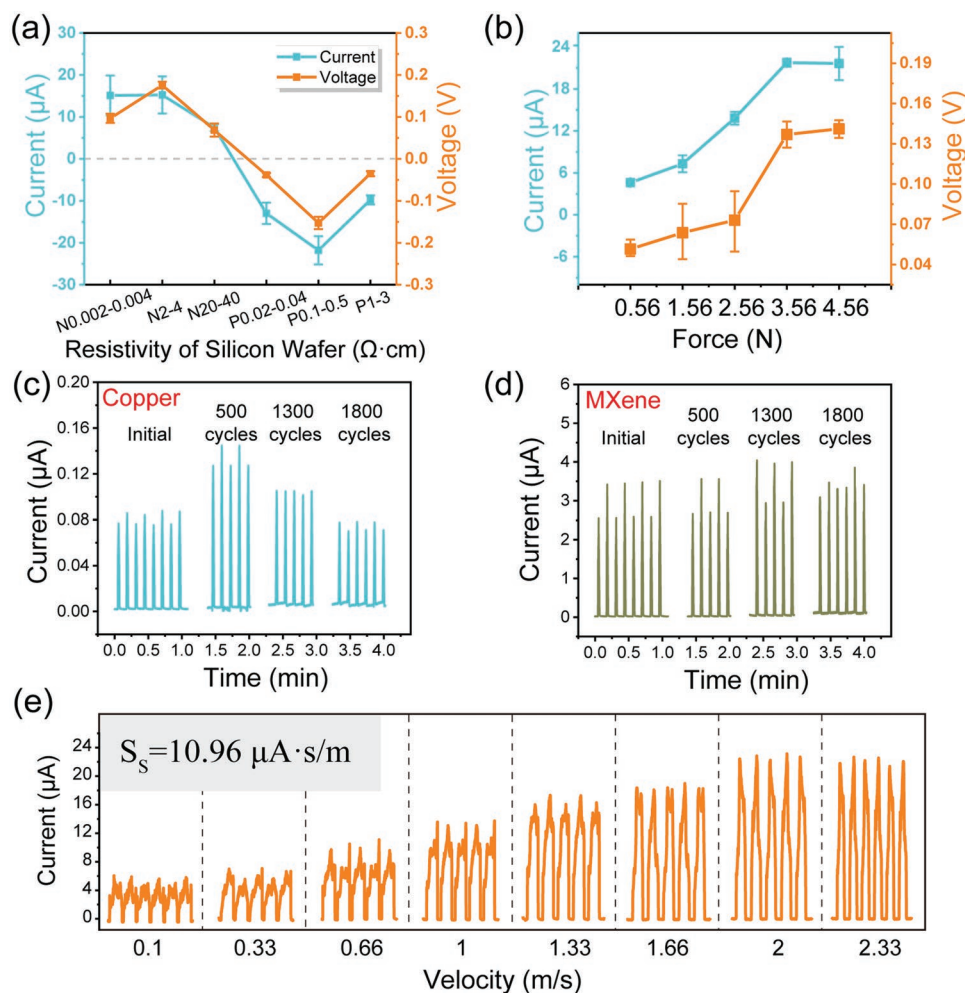


Figure 3. The electrical output (open-circuit voltage and short-circuit current) performance of the MS-TVNG. a) The output of using different types and resistivities of silicon wafers. b) The output voltage and current generated by applying different normal forces, perpendicular to the friction interface. c–d) Durability of the Cu-based (c) and MXene-based (d) TVNGs tested for various cycles. e) The output performance of the MS-TVNG generated by applying different sliding speeds.

the sliding process and stays in the sliding traces, resulting in the sliding friction becoming into a rolling friction. The other one is that the MXene nanosheets are more prone to interlayer slip due to their layered structures, endowing them excellent lubricating properties as previously reported.^[20]

To further explore the parameters that control the behavior of the MS-TVNG, the types and resistivities of silicon wafers, the applied pressure, and the sliding velocity are varied to study their influence on the electrical output (Figure 3). First, the direction of the electrical signal appears to be opposite for different types of silicon wafers (Figure 3a). Taking MXene and N-type silicon TVNG for example, with the increase of doping concentration, the higher Fermi level of electron filling will generate a stronger built-in electric field, which promotes the drifting transport of carriers. However, when the doping concentration reaches a certain amount, the transport of the carriers is strongly scattered by the doped impurities. These result in that the output current/voltage first increases and then decreases with the decrease of the resistivity of the silicon wafers. Noting that the higher the doping concentration is, the

higher the resistivity will be. Under a normal force of 4.56 N and a sliding speed of 2 m s^{-1} , the maximum output current and voltage are $-22 \mu\text{A}$ and -140mV , respectively, for a P-type silicon wafer with a resistivity of 0.1–0.5 $\Omega\text{-cm}$ (Figure 3a and Figure S3, Supporting Information). Second, the output of the MS-TVNG is enhanced by increasing pressure for a P-type (0.1–0.5 $\Omega\text{-cm}$) silicon wafer under a sliding speed of 2 m s^{-1} (Figure 3b), which is due to the greater release of residual bond formation energy obtained by carriers when force increases, and hence resulting in an increased number of carriers. Third, the durability test (under conditions of 2.56 N, 2 m s^{-1} , and N-type (20–40 $\Omega\text{-cm}$) silicon wafer) results of the Cu-based and MXene-based TVNGs are shown in Figure 3c,d and Figure S4, Supporting Information, where both TVNGs worked for more than 210 min. The current for the Cu-based TVNG was increasing and then decreasing over time. The gradually increased contacting area of the Cu film at the very beginning might lead to an increase in current, while the damaged surface of Si wafer might result in decreasing current. In contrast, the current of the MS-TVNG is higher, more stable and

even exhibits a slight increase with time, revealing its superior wear-resistance and stability. Furthermore, the DC current of the MS-TVNG increases almost linearly with the increase of sliding speed (Figure 3e), and a sensitivity, S_S , of $10.96 \mu\text{A s m}^{-1}$ is achieved for a P-type ($0.1\text{--}0.5 \Omega \cdot \text{cm}$) silicon wafer under a normal force of 4.56 N . From these observations, using MS-TVNG for applications in self-powered force and speed sensing is more promising.

Concerning the mechanism, we consider that when a metal MXene is in contact with an N-type silicon wafer, due to the difference in work functions of the two materials, a redistribution of carrier concentration at the interface occurs, giving birth to a built-in electric field. A Schottky barrier is formed in the depletion region of the N-type silicon.^[5a,21] However, it is worth mentioning the Schottky theory has not yet been confirmed in

most practical cases, owing to complex surface states such as surface dangling bonds, surface reconstruction or relaxation, steps and kinks, non-stoichiometric vacancies, and impurity atom adsorption.^[5a,22] Due to the large surface states, the metal/semiconductor interface forms a Schottky barrier easily no matter if there is a difference in work functions. A schematic of the external circuit and the corresponding band structure under thermal equilibrium (static state) are shown in Figure 4a. Since no extra energy is released at the static state, there is no output current. When a piece of MXene film starts sliding on the N-type silicon, a positive DC current is detected due to the tribovoltaic effect (Figure 4b).^[11,23] The sliding kinetic energy breaks the bonds at the interface, and then newly formed bonds release bindingtons which are absorbed by a large number of electrons trapped in the surface states. As a result, the surface

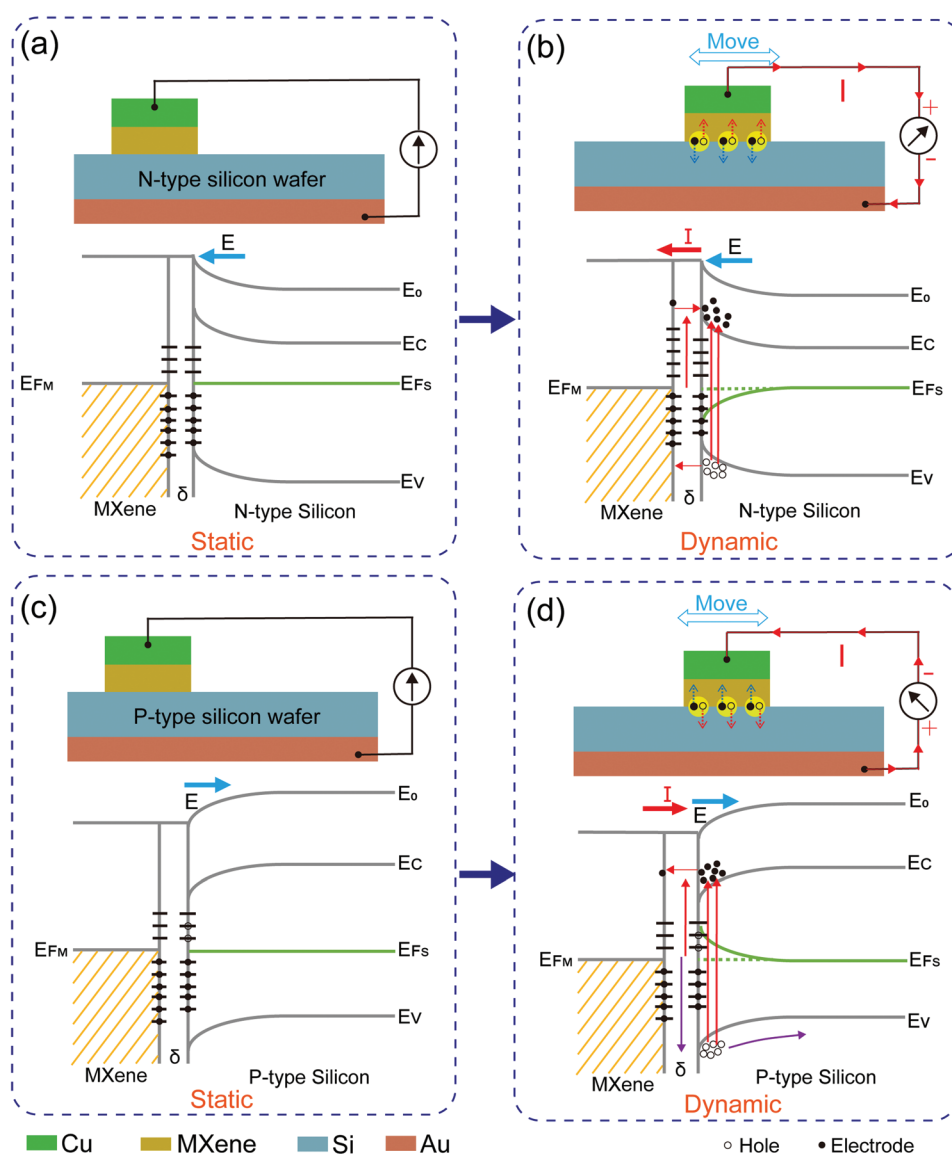


Figure 4. Schematic diagrams of the working principle and corresponding energy band structure of the MS-TVNG. a,b) The schematic diagrams denoting charge transfer between an MXene and an N-type silicon wafer under static state (a) and dynamic state (b), respectively. c,d) The schematic diagrams of charge transfer between an MXene and a P-type silicon wafer under static state (c) and dynamic state (d), respectively.

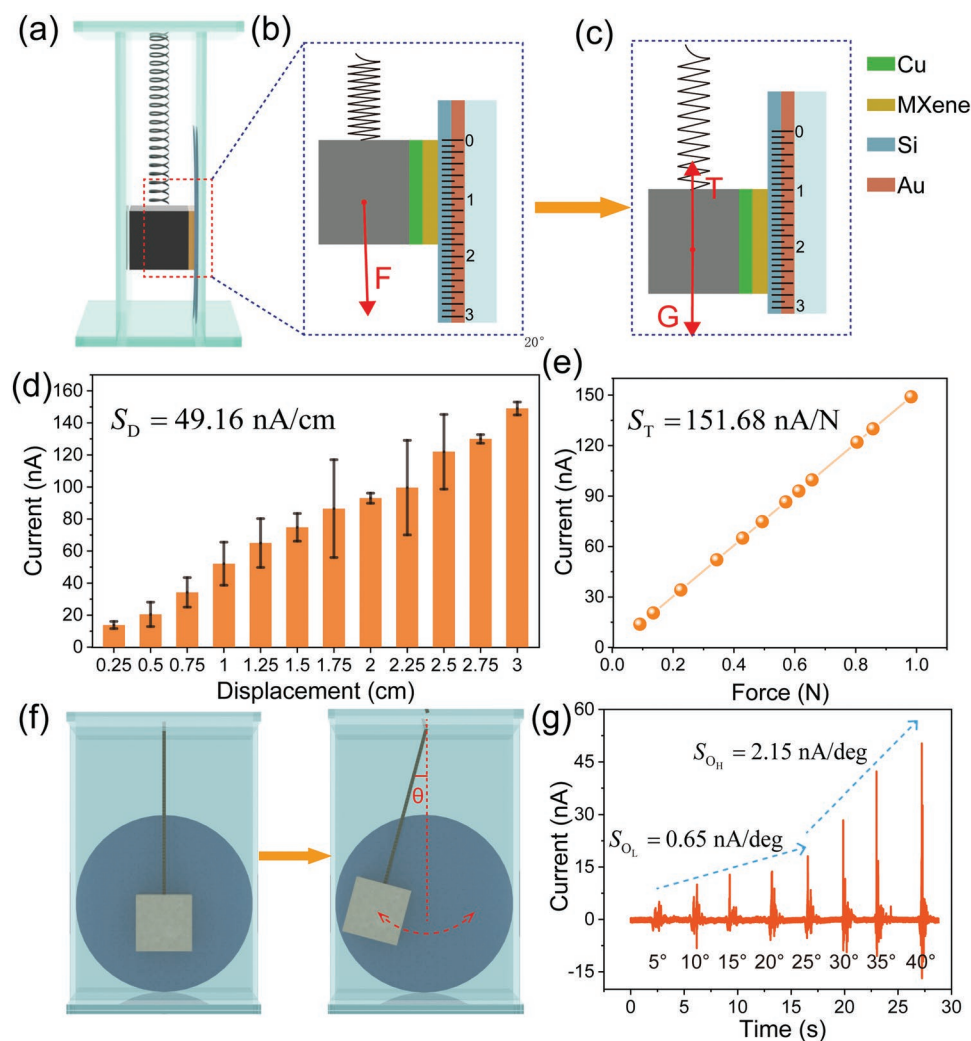


Figure 5. Applications of the MS-TVNG in self-powered sensing. a) Schematic of the device structure for displacement and force sensing. b,c) Schematic diagrams of force analysis of the external force acting on the slider (b) and being released (c). d) The amplitude of output current of the MS-TVNG when the slider is stretched to a different displacement and then released. e) The changing curve between the output current and tensile force. f) Schematic diagram of the MS-TVNG for vibration sensing and an indication for oscillation angle. g) The output current as a function of different oscillation angles.

electrons are driven to the bulk of the N-type silicon due to the built-in electric field. Furthermore, the bindingtons released by newly formed bonds can also excite electrons and holes at the depletion region of the N-type silicon. These principles can explain why the greater the pressure and the sliding speed, the greater the output current. Compared with the N-type silicon case, the energy band of the Schottky barrier of the MXene and P-type silicon junction bends downward. Similarly, there is no current under a static state, as shown in Figure 4c. When a piece of MXene film slides on the P-type silicon wafer, electrons and holes in the surface states as well as in the depletion region will be induced after absorbing the bindingtons released when new bonds are formed, resulting in a negative current due to the opposite direction of the built-in electric field compared with that of the case of N-type silicon (Figure 4d).

As shown in Figure 5, owing to the properties of MXene and the working principles of TVNGs, the MS-TVNG can produce accurate, continuous and real-time electrical DC signals

that not only exploitable for self-powered speed sensors but also have great application potential in high-performance displacement, tension, oscillation angle, and vibration sensing. This was demonstrated by the fabrication of a multifunctional sensor. A schematic of the multifunctional sensor's structure is shown in Figure 5a. The detailed fabrication processes of this sensor can be found in the Experimental Section. The specific enlarged views are shown in Figure 5b,c. The spring can convert external mechanical energy into potential energy to produce a long-lasting output. The sensitivities of the sensor, S_X , can be calculated by the following formula:

$$S_X = \frac{\Delta I}{\Delta x} \quad (1)$$

where the X (X = S, D, T, O_H, and O_L for sensors of speed, displacement, tensile force, oscillation at higher angles, and oscillation at lower angles, respectively) is a unified code name, ΔI

is the change in current with the change of independent variable, and Δx is the change of independent variable.

First, the current output is proportional to the relative sliding speed of the slider as illustrated in Figure 3e. Therefore, the sliding speed of the slider can be adjusted, which allows its use as a speed sensor with a sensitivity of $10.96 \mu\text{A s m}^{-1}$. Second, the device can act as a displacement sensor. Using an external force F to pull the sliding block to different distances (displayed on the scale ruler next to the sliding block), the sliding block acquires different elastic potential energies (Figure 5b). After the force F is removed, the slider receives the elastic force of the spring and its own gravity, and the elastic potential energy of the spring is converted into the kinetic energy of the slider movement (Figure 5c). The friction energy loss between the slider and the silicon wafer will bring the slider to a standstill state after several up and down cycles. Correspondingly, the slider feels different elastic potential energy when stretched to different distances, so the initial speed of the slider will be different when it is released. According to the principle depicted with the current output of the MS-TVNG, the current increases as the sliding speed increases. It can also be inferred that the stretching distance is proportional to the output current. Even if the minimum displacement interval is 0.25 cm, the device with a sensitivity (S_D) of 49.16 nA cm^{-1} can still provide a good linear relationship to displacement and current, proving the reliability of the device as a displacement sensor (Figure 4d and Video S1, Supporting Information). Third, the device can also work as a tension sensor. Detailed discussion about the MS-TVNG used as a tension sensor can be found in the Supplementary Text (Supporting Information). The relationship between the external force acting on the slider and the current output can be written as

$$F = -\Delta F' = ka\Delta I \quad (2)$$

where F is the tensile force, F' is the tensile force of the spring, k is the elastic coefficient of the spring, a is a constant, and I is the output current of the MS-TVNG. The relationship between the measured tensile force and the elongation of the spring is shown in the Supplementary Text and Figure S5, Supporting Information, where the elastic coefficient k can be calculated. According to the relationship, the change of the MS-TVNG's output current, ΔI , should be proportional to the tensile force. The experimentally observed linear relationship between the calculated tensile force and the measured current demonstrates the feasibility of using the output current to construct a tensile force sensor with sensitivity, S_T , of 151.68 nA/N (Figure 5e). In addition, by replacing the spring with a fixed rope, the device can be regarded as a simple pendulum structure (Figure 5f). As the swing amplitude changes (θ is changed), the maximum speed of the pendulum also changes. Therefore, the device can work as an oscillation sensor. Under different simulated environmental oscillation angles, the output current increases linearly with the increasing of the oscillation amplitude, as shown in Figure 5g and Video S2, Supporting Information. Especially, it is more sensitive with a sensitivity of 2.15 nA/deg at higher oscillation angles ($>25^\circ$) compared to that (0.65 nA/deg) at lower angles. It is worth noting that the negative signals are derived from the noises from the test system, which have little

effect on the sensing performance. Moreover, when the sensor is placed on a horizontal support, it can respond to environmental vibrations, such as knocking on the support with a random force (Figure S6a, Supporting Information). Since the force of each tap is different, the vibrational amplitude generated by the bracket varies, which transfers to random current output signals (Figure S6b, Supporting Information). It should be noted that the sensor can separately realize speed, displacement, tension, oscillation angle, and vibration sensing by controlling related variables according to the given mechanical stimulus, but it can hardly identify multiple physical quantities simultaneously due to the intercoupled quantities.

3. Conclusion

In summary, the unique metal property of the MXene is utilized to generate real-time DC current by sliding on a silicon wafer based on the tribovoltaic effect. The output current of the MS-TVNG can reach up to 30 times compared to that of the traditional Cu-based TVNG. Moreover, the silicon wafer doping types, the pressure between the two friction surfaces, and the sliding speed of the slider have a significant influence on the output performance of the MS-TVNG. Besides, thanks to the layered structure of MXene, the MS-TVNG possesses obvious superior features in terms of wear-resistance and stability, even after 210 min of continuous work. Considering the current of the MS-TVNG is proportional to the sliding speed, new principles for speed, displacement, tension, oscillation angle, and vibration sensors are proposed. These are exciting results unveiling great opportunities for the research and engineering of new devices based on MS-TVNGs' principles.

4. Experimental Section

MXene Film Preparation: The MXene ($\text{Ti}_2\text{C}_3\text{Tx}$) black powder was purchased from Jiangsu XFANO materials Tech Co., Ltd., whose specifications are multilayered nanosheets, of a thickness of 100–200 nm, and a purity of 54–68 wt%. The MXene film was prepared by a tableting method. First, in order to obtain an MXene film with a uniform thickness, 40 mg of MXene powder was divided into equal parts (usually four parts), and then the powders was poured onto the conductive copper tape (dimension $1.5 \text{ cm} \times 1.5 \text{ cm}$) that were evenly marked into four equal parts, and a spoon was used to spread the powder evenly on the surface of the tape. Then the copper tape with MXene was transferred to the tablet press machine and kept under a pressure of 25 MPa for 5 min to ensure the MXene adhered firmly to the surface of the copper sheet.

Fabrication of the MS-TVNG: The silicon wafers with different doping concentrations were purchased from Suzhou Jinggui Technology Co., Ltd., whose specifications are 4 in., crystal plane orientation along [100], a diameter of $100 \pm 0.3 \text{ mm}$, and a thickness of $500 \pm 25 \mu\text{m}$. First, the silicon wafers were soaked in 10% hydrofluoric acid for 5 min to remove the surface oxide layer and then cleaned by the alcohol and deionized water in turns. Second, the Au film layer (50 nm) was coated on the matte side of the silicon wafer as a bottom electrode via magnetron sputtering process (Denton Discovery 635, Ar gas environment, 10 min). Then, the MXene film was pasted on the acrylic board. Finally, the bottom and top electrodes were connected using Cu wires.

Fabrication of the Multifunctional Sensor Based on the MS-TVNGs: First, a shell bracket made of plexiglass acrylic was laser-cut, and then two pieces of horizontal and two pieces of vertical acrylic plates were glued

to each other with a connection angle set to be 90°. The two vertical acrylic plates were parallel to each other to ensure that the sliders could glide steadily in the middle. Next, one end of the spring was fixed on the top acrylic plate, and the lower end was connected to the slider. An iron block after insulation treatment was used to increase the elastic potential energy of the spring and enhance the sensitivity of the sensor. Then, the two parts of the MS-TVNG were glued on the bracket and the sliding block, respectively. Finally, a ruler was glued to the edge of a vertical acrylic so the displacement can be easily read.

Material Characterization and Electrical Measurement of the MS-TVNGs: A Keithley 6514 electrometer and a Keithley 6510 digital multimeter were used to measure the output electric signals of the MS-TVNGs. If no special declaration, the area of the upper copper electrode was set to be $1.5 \times 1.5 \text{ cm}^2$. The XRD pattern was measured with an X-ray diffractometer (XPert3 Powder, Netherlands) with a voltage of 40 kV, a current of 40 mA, a step length of 0.02° , and a scanning speed of 0.5° s^{-1} . The Raman spectra were recorded with a laser confocal Raman spectrometer (LabRAM HR Evolution) equipped with a $\times 50$ objective lens, a 532 nm laser, and a grating of 1800 gr mm^{-1} . Bright field TEM images were acquired using a Thermo Fisher Tecnai F20 FEG TEM at 200 kV. Energy dispersive X-ray spectroscopic (EDX) mapping was conducted using a Thermo Fisher Themis-Z S/TEM at 300 kV equipped with a Super-X EDS detector system consisting of four silicon drift detectors with $50 \mu\text{s}$ pixel dwell time and summed over 35 frames. The MXene films were characterized with a scanning electron microscopy (Nova NanoSEM 450) by applying a 10 kV acceleration. The images of scratches on the silicon wafers were obtained with an optical microscope (ZEISS Axio Imager M2m). The pressures between the two friction surfaces were recorded by a pressure sensor (SIMBATOUCHE SBT674), whose maximum range and accuracy are 100 and 0.01 N, respectively.

Supporting Information

Supporting Information is available from the Wiley Online Library or from the author.

Acknowledgements

This research was supported by the National Key R & D Project from Minister of Science and Technology (2021YFA1201601) and the National Natural Science Foundation of China (Grant No. 52192610). The authors also thank Xiang Zhang and Fengying Jiang for the assistance in experiment.

Conflict of Interest

The authors declare no conflict of interest.

Data Availability Statement

The data that support the findings of this study are available from the corresponding author upon reasonable request.

Keywords

direct-current, MXene, self-powered sensors, speed sensing, tribovoltaic nanogenerators

Received: December 22, 2021

Revised: February 8, 2022

Published online:

- [1] a) Z. L. Wang, *Adv. Energy Mater.* **2020**, *10*, 2000137; b) C. Wu, A. C. Wang, W. Ding, H. Guo, Z. L. Wang, *Adv. Energy Mater.* **2019**, *9*, 1802906; c) L. Zhou, D. Liu, J. Wang, Z. L. Wang, *Friction* **2020**, *8*, 481.
- [2] a) Z. L. Wang, *Rep. Prog. Phys.* **2021**, *84*, 096502; b) W. Liu, Z. Wang, G. Wang, G. Liu, J. Chen, X. Pu, Y. Xi, X. Wang, H. Guo, C. Hu, Z. L. Wang, *Nat. Commun.* **2019**, *10*, 1426.
- [3] a) R. Yang, R. Xu, W. Dou, M. Benner, Q. Zhang, J. Liu, *Nano Energy* **2021**, *83*, 105849; b) Q. Zhang, K. Barri, S. R. Kari, Z. L. Wang, A. H. Alavi, *Adv. Funct. Mater.* **2021**, *31*, 2105825; c) W. G. Kim, D. W. Kim, I. W. Tcho, J. K. Kim, M. S. Kim, Y. K. Choi, *ACS Nano* **2021**, *15*, 258.
- [4] Z. Zhao, L. Zhou, S. Li, D. Liu, Y. Li, Y. Gao, Y. Liu, Y. Dai, J. Wang, Z. L. Wang, *Nat. Commun.* **2021**, *12*, 4686.
- [5] a) Z. Zhang, D. Jiang, J. Zhao, G. Liu, T. Bu, C. Zhang, Z. L. Wang, *Adv. Energy Mater.* **2020**, *10*, 1903713; b) Z. Zhang, T. He, J. Zhao, G. Liu, Z. L. Wang, C. Zhang, *Mater. Today Phys.* **2021**, *16*, 100295; c) S. Lin, Y. Lu, S. Feng, Z. Hao, Y. Yan, *Adv. Mater.* **2019**, *31*, e1804398.
- [6] a) R. Xu, Q. Zhang, J. Y. Wang, D. Liu, J. Wang, Z. L. Wang, *Nano Energy* **2019**, *66*, 104185; b) Y. Lu, Z. Hao, S. Feng, R. Shen, Y. Yan, S. Lin, *iScience* **2019**, *22*, 58.
- [7] J. Meng, Z. H. Guo, C. Pan, L. Wang, C. Chang, L. Li, X. Pu, Z. L. Wang, *ACS Energy Lett.* **2021**, *6*, 2442.
- [8] J. Liu, M. I. Cheikh, R. Bao, H. Peng, F. Liu, Z. Li, K. Jiang, J. Chen, T. Thundat, *Adv. Electron. Mater.* **2019**, *5*, 1900464.
- [9] a) M. Zheng, S. Lin, Z. Tang, Y. Feng, Z. L. Wang, *Nano Energy* **2021**, *83*, 105810; b) Y. Lu, Y. Yan, X. Yu, X. Zhou, S. Feng, C. Xu, H. Zheng, Z. Yang, L. Li, K. Liu, S. Lin, *Research* **2021**, *2021*, 7505638.
- [10] J. Liu, A. Goswami, K. Jiang, F. Khan, S. Kim, R. McGee, Z. Li, Z. Hu, J. Lee, T. Thundat, *Nat. Nanotechnol.* **2018**, *13*, 112.
- [11] Z. L. Wang, A. C. Wang, *Mater. Today* **2019**, *30*, 34.
- [12] a) Y. C. Dong, S. S. K. Mallineni, K. Maleski, H. Behlow, V. N. Mochalin, A. M. Rao, Y. Gogotsi, R. Podila, *Nano Energy* **2018**, *44*, 103; b) H. C. Fu, V. Ramalingam, H. Kim, C. H. Lin, X. Fang, H. N. Alshareef, J. H. He, *Adv. Energy Mater.* **2019**, *9*, 1900180; c) C. M. Jiang, C. Wu, X. J. Li, Y. Yao, L. Y. Lan, F. N. Zhao, Z. Z. Ye, Y. B. Ying, J. F. Ping, *Nano Energy* **2019**, *59*, 268.
- [13] a) M. Naguib, M. Kurtoglu, V. Presser, J. Lu, J. Niu, M. Heon, L. Hultman, Y. Gogotsi, M. W. Barsoum, *Adv. Mater.* **2011**, *23*, 4248; b) M. Naguib, V. N. Mochalin, M. W. Barsoum, Y. Gogotsi, *Adv. Mater.* **2014**, *26*, 992; c) A. Agresti, A. Pazniak, S. Pescetelli, A. Di Vito, D. Rossi, A. Pecchia, M. Auf der Maur, A. Liedl, R. Larciprete, D. V. Kuznetsov, D. Saranin, A. Di Carlo, *Nat. Mater.* **2019**, *18*, 1228; d) A. VahidMohammadi, J. Rosen, Y. Gogotsi, *Science* **2021**, *372*, eabf1581.
- [14] M. Malaki, R. S. Varma, *Adv. Mater.* **2020**, *32*, e2003154.
- [15] X. Wu, Z. Wang, M. Yu, L. Xiu, J. Qiu, *Adv. Mater.* **2017**, *29*, 1607017.
- [16] a) W. T. Cao, H. Ouyang, W. Xin, S. Y. Chao, C. Ma, Z. Li, F. Chen, M. G. Ma, *Adv. Funct. Mater.* **2020**, *30*, 2004181; b) Y. Xie, P. R. C. Kent, *Phys. Rev. B* **2013**, *87*, 235441; c) L. Yin, Y. Li, X. Yao, Y. Wang, L. Jia, Q. Liu, J. Li, Y. Li, D. He, *Nano-Micro Lett.* **2021**, *13*, 78; d) Y. Z. Zhang, J. K. El-Demellawi, Q. Jiang, G. Ge, H. Liang, K. Lee, X. Dong, H. N. Alshareef, *Chem. Soc. Rev.* **2020**, *49*, 7229.
- [17] a) T. B. Limbu, B. Chitara, M. Y. Garcia Cervantes, Y. Zhou, S. Huang, Y. Tang, F. Yan, *J. Phys. Chem. C* **2020**, *124*, 17772; b) M. Salauddin, S. M. S. Rana, M. Sharifuzzaman, M. T. Rahman, C. Park, H. Cho, P. Maharjan, T. Bhatta, J. Y. Park, *Adv. Energy Mater.* **2020**, *11*, 2002832.
- [18] Z. Hao, T. Jiang, Y. Lu, S. Feng, R. Shen, T. Yao, Y. Yan, Y. Yang, Y. Lu, S. Lin, *Matter* **2019**, *1*, 639.
- [19] X. Huang, X. Xiang, J. Nie, D. Peng, F. Yang, Z. Wu, H. Jiang, Z. Xu, Q. Zheng, *Nat. Commun.* **2021**, *12*, 2268.

- [20] a) A. Rodriguez, M. S. Jaman, O. Acikgoz, B. Wang, J. Yu, P. G. Grutzmacher, A. Rosenkranz, M. Z. Baykara, *Appl. Surf. Sci.* **2021**, 535, 147664; b) X. H. Zhang, M. Q. Xue, X. H. Yang, Z. P. Wang, G. S. Luo, Z. D. Huang, X. L. Sui, C. S. Li, *RSC Adv.* **2015**, 5, 2762.
- [21] a) Y. Lu, Q. Gao, X. Yu, H. Zheng, R. Shen, Z. Hao, Y. Yan, P. Zhang, Y. Wen, G. Yang, S. Lin, *Research* **2020**, 2020, 5714754; b) L. H. Xu, T. Wu, P. R. C. Kent, D. E. Jiang, *Phys. Rev. Mater.* **2021**, 5, 054007.
- [22] a) M. Zheng, S. Lin, L. Xu, L. Zhu, Z. L. Wang, *Adv. Mater.* **2020**, 32, e2000928; b) Y. Wang, G. Zhang, H. Wu, B. Sun, *Adv. Energy Mater.* **2021**, 11, 2100578.
- [23] Y. Song, N. Wang, Y. Wang, R. Zhang, H. Olin, Y. Yang, *Adv. Energy Mater.* **2020**, 10, 2002756.